THE JOURNAL OF PHYSICAL CHEMISTRY B

Article

pubs.acs.org/JPCB

Multiscale Simulation on a Light-Harvesting Molecular Triad

Guoxiong Su,[†] Arkadiusz Czader,[‡] Dirar Homouz,[§] Gabriela Bernardes,[†] Sana Mateen,[†] and Margaret S. Cheung*[,†]

[†]Department of Physics, University of Houston, Houston, Texas 77204, United States

[‡]Department of Chemistry, University of Houston, Houston, Texas 77204, United States

[§]Department of Applied Math and Sciences, Khalifa University, Abu Dhabi, United Arab Emirates

Supporting Information

ABSTRACT: We have investigated the effect of solvation and confinement on an artificial photosynthetic material, carotenoid-porphyrin-C_{60} molecular triad, by a multiscale approach and an enhanced sampling technique. We have developed a combined approach of quantum chemistry, statistical physics, and all-atomistic molecular dynamics simulation to determine the partial atomic charges of the ground-state triad. To fully explore the free energy landscape of triad, the replica exchange method was applied to enhance the sampling efficiency of the simulations. The confinement effects on the triad were modeled by imposing three sizes of spherocylindrical nanocapsules. The triad is structurally flexible under ambient conditions, and its conformation distribution is manipulated by the choice of water models and confinement. Two types of water models (SPC/E and TIP3P) are used for solvation. When solvated by SPC/E water, whose HOH angle follows an ideal tetrahedron, the structural characteristics of triad is compact in the bulk systems. However, under a certain nanosized confinement that drastically disrupts hydrogen bond networks in solvent, the triad favors an extended configuration. By contrast, the triad solvated by TIP3P water shows a set of U-shaped conformations in the confinement. We have shown that a slight structural difference in the two water models with the same dipole moment can have great distinction in water density, water orientation, and the number of hydrogen bonds in the proximity of a large flexible compound such as the triad. Subsequently, it has direct impact on the position of the triad in a confinement as well as the distribution of conformations at the interface of liquid and solid in a finite-size system.

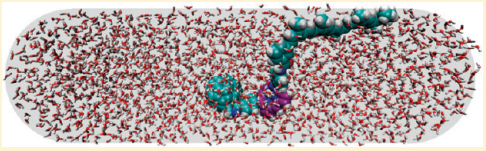

I. INTRODUCTION

The amount of energy that humans use every year is about the amount of energy delivered to the Earth by the Sun in just one hour.[1−3] This is equivalent to 1.2×10^5 TW, and it easily exceeds the rate at which all of the man-made machines can produce and use, which is about 13.5 TW.[2,3] However, currently, less than 0.1% of world electricity is converted from the Sun.[3] The difficulty in harvesting solar energy lies in the fact that, unlike fossil fuels, sunlight spreads out over a large area and it is hard to harness its energy in high concentration using current available technology. Therefore, there is a need for more efficient ways to convert solar energy. The technology for better efficiency can be greatly enhanced by learning from natural light-harvesting systems, such as plants and bacteria, which show an impressive efficiency for converting and storing solar energy. One of the several bioinspired materials was first synthesized by the Gust group[4] for the investigation of efficient photovoltaic properties. This material is a donor−acceptor triad system composed of a covalently linked fullerene molecule (C_{60}), a diarylporphyrin (P), and a carotenoid polyene (C). In Gust's experiments on the triad, the porphyrin was excited by a pulsed laser with a wavelength in the range of yellow-orange visible light (590 nm) to give C−^{1}P−C_{60}. This state decays by photoinduced electron transfer to the C_{60} (i.e., C−$P^{\bullet+}$−$C_{60}^{\bullet-}$). Subsequently, the carotenoid donates one electron to the porphyrin. In the final charge-separated state, an excited electron on the C_{60} and a hole on the carotenoid (i.e., $C^{\bullet+}$−P−$C_{60}^{\bullet-}$), it was found that this state has a long-lived lifetime of hundreds of nanoseconds at ambient temperature in organic solvents such as 2-methyltetrahydrofuran (MTHF) and benzonitrile (BZN). It is further quenched to a triplet state of C (i.e., ^{3}C−P−C_{60}) with a lifetime of several microseconds by charge recombination, before reaching its ground state (C−P−C_{60}).

The triad, however, is still far from being utilized in real-world applications. In 2003, the Gust group measured the dipole moment of the triad's charge-separated state in MTHF by applying a transient direct current (dc) photocurrent method and showed that it forms a large dipole moment in excess of 150 D.[5] It has potentially become a desirable molecular-scale optoelectronic device[6] as its lifetime can be increased by 50% in the presence of an external magnetic field at low temperatures.[7] This large dipole moment is thought to be valid only if a linear conformation for the triad is assumed. However, conformational changes in the triad were probed under ambient conditions when the triad was mixed with BZN/Triton X-100

Special Issue: Macromolecular Systems Understood through Multiscale and Enhanced Sampling Techniques

Received: December 20, 2011
Revised: February 10, 2012
Published: February 22, 2012

"reverse" micelles in aqueous solutions.[8] When the triad is inside a micelle, it appears to be in a "folded" conformation that can lead to a smaller value of dipole moment (110 D) estimated by a quantum chemistry calculation. It is suggested that flexibility in a triad is important to its dynamics in solvents, and this can be challenging for using the triad in real-world applications.

The study of the triad and its ability to maintain a large dipole moment in real-world applications is an exciting area that has attracted the attention of many computational chemists in their pursuit of a better design for solar energy harnessing materials. Baruah and Pederson[9] first applied density functional theory (DFT) to study its ground state in its elbow shaped and linear geometry. Later, they reported another study on the triad in its excited states by incorporating a time-dependent DFT method.[10] They have also studied the charge-transfer dynamics[11] by running kinetic Monte Carlo simulations. However, these studies are based on a static configuration of the triad in its extended state. There is no investigation regarding the impact of thermal fluctuation on both the triad and solvent: the changes of the latter will affect the former, while solvent polarization is crucial in reordering the excite-state energies and the charge-separation process of the triad.

We aim to fill the knowledge gap of the molecular dynamics (MD) of the triad, a large and flexible structure, in solvent by using MD simulations. As a first step, we have investigated the conformational distribution of the triad in its ground state. One of the biggest challenges in studying the triad, however, is how to determine the electronic charges of its atoms for the computation of Coulomb electrostatic interactions that cannot be experimentally measured. Many approaches have been employed for calculations of atomic charges either based on quantum mechanically derived wave function[12−14] or obtained by fitting atom-centered monopoles to the molecular electrostatic potential (MEP).[15−18] While, quantum mechanics offers the easiest methods of calculating the charges, none of the existing procedures for computing atomic charges is universally agreed upon. Different methods of charge derivation based on quantum mechanical calculations will give charges capable of reproducing certain molecular properties, but none of these charge models have been proven satisfactory in all regards.[18−20] Moreover, the quantum mechanical calculations are usually carried out for a single configuration at 0 K in the gas phase, causing additional complications when atomic charges change with different conformations of the molecule.[21,22] This is especially important in MD simulations when extensive regions of conformational space are sampled, but the atomic charges employed are calculated based on a single geometry.

Motivated by the fact that the triad is very flexible at ambient temperatures and the atomic charges depend on conformations, we have combined a statistical physics approach to compute ensemble-averaged charges of conformations selected from the energy landscape of a triad and quantum chemistry calculations to compute charges[23] for each selected conformation. All-atomistic structures of the triad were sufficiently sampled according to Metropolis criteria[24] from an NVT ensemble, and then the charges of each structure were computed using several quantum chemistry methods, followed by a procedure that averaged charges over these structures. The ensemble-averaged charges were introduced in the Hamiltonian for the computation of Coulomb electrostatic interaction in regard to MD simulations. We have adopted three different quantum chemistry approaches for the calculation of the atomic charges, including the RESP, the AM1-BCC, and Mulliken charges. They were compared with the electrostatic potential (ESP) charges obtained for a static structure optimized at DFT level.[25] The best set of charges of the triad is the one capable of representing the energetics of the ground state C−P−C_{60} triad; however, lack of experimental data poses a significant obstacle in using this criterion for selecting the partial charges. After careful comparison of the of the magnitudes of the charges, their conformational dependability and the time required for their computations, we have chosen the AM1-BCC as the quantum chemistry approach for the computation of the charges for the selected triad structures.

To probe the solvent configurations surrounding the triad, we have used two well-studied water models, TIP3P and SPC/E, as solvents as a first step to probe their effect. Although both are single point charge, three-site models, the parameters for the SPC/E model include an ideal tetrahedral angle on the HOH angle. We have further simulated the triad in various nanosizes of spherocylindrical confinement (SC), to characterize the confinement effect on the configurations of a triad as well as surrounding water molecules at the liquid−solid interface, which can provide insight for the manipulation of large and complex molecules under ambient conditions.[26,27] To achieve sufficient sampling of the triad configuration and solvent in such large systems, we have incorporated the replica exchange method,[28] which effectively integrates with high-performance computing resources.

These investigations allow us to characterize the confinement effect on the distribution of the triad configurations, the position of the triad in the confinement, the water density, and the hydrogen bonding of water molecules surrounding this topologically complex molecule. Although we have yet to investigate the charge-separated state of the triad in organic solvents, this study is valuable because it is the first study to explore the energy landscape of a large, flexible bioorganic molecule in a confinement by integrating the approach of quantum chemistry and all-atomistic MD simulations. This work has built a foundation for future studies on other bioorganic compounds involving polyconjugates in liquid and condense phases.

II. METHODS SECTION

II.1. Sample Preparation. The coordinates of the triad of an extended configuration were computed *in vacuo* by Baruah and Pederson.[9] The set of charges for this structure was computed using the fitted charges from the electrostatic potential derived from DFT calculation,[25] and they are shown in Figure 2D. The atom indices are shown in Table S1 (Supporting Information). Its two-dimensional (2-D) chemical structure and three-dimensional (3-D) representation are illustrated in Figure 1A,B, respectively. We have computed a set of thermally averaged charges of triad using a novel multiscale method involving an integration of methods of quantum chemistry calculations (femtosecond scale) and MD simulations (submicrometer second scale). Procedures are below:

(1). Initial Conditions. The parameters for the structural Hamiltonian were generated by Antechamber, one of the modules in AmberTools 1.4,[29] using a General AMBER Force Field (GAFF)[30] while the initial charges were taken from Baruah's calculation based on a single extended conformation.[25]

(2). Molecular Dynamics. The triad was solvated with TIP3P water in a cubic periodic boundary box (10 nm ×10 nm ×10 nm).

dx.doi.org/10.1021/jp212273n | J. Phys. Chem. B 2012, 116, 8460−8473

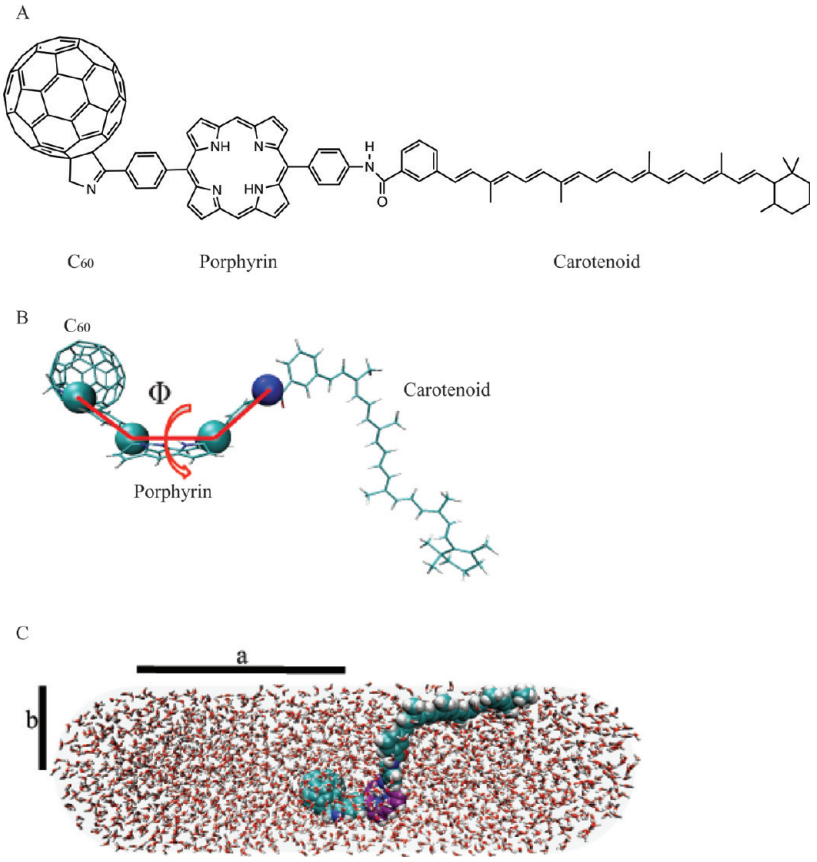

Figure 1. (A) A 2-D chemical diagram of the triad. (B) A 3-D representation of the triad. A scheme of Φ, which is the pseudodihedral angle defined by four atoms, whose indices are 60, 75, 93, and 121, respectively. (C) A snapshot of an all-atomistic representation of the triad solvated in an SC, which is defined by the half-length of a central cylinder, *a*, and the radius of a hemisphere, *b*. *a* is 3.65 nm and *b* is 1.61 nm in the figure. Atoms are colored by their types: hydrogen in white, carbon in cyan, nitrogen in blue, and oxygen in red. The carbon atoms of porphyrin are colored in purple for visual guidance.

The solvated triad was then equilibrated at 300 K, followed by replica exchange molecular dynamics (REMD)[28,31] simulations to generate a 20-ns trajectory for each temperature ranging from 280 to 400 K. A free energy landscape as a function of the first two principal components (PC1 and PC2) from the principal component analysis (PCA)[32] was obtained at 350 K, at which the structural variations of triad can be better sampled than at a lower temperature 300 K. We have selected 1000 representative structures for producing an ensemble average by using Metropolis criteria[24,33] dependent on a potential energy difference between a randomly selected structure in this ensemble and the structure with the lowest free energy in the free energy landscape from an ensemble at T = 350 K.

(3). Quantum Chemistry Calculation. The atomic charges for 207 atoms in each of the 1000 representative structures of the triad were calculated using three different methods: Mulliken population analysis,[12] restrained electrostatic potential (RESP),[15−18] and AM1-BCC.[34,35] The resulting charges obtained with each method were subsequently averaged over all 1000 structures of the ensemble average. The Mulliken population analysis was carried out at the B3LYP/6-31G(d) level using NWCHEM.[36] The second set of charges, RESP charges, were fitted to the MEP calculated at the B3LYP/6-31G(d) level of theory. The MEP was sampled using a cubic grid of density 0.3 Å, and default value, 0.001 au, for hyperbolic restraints was used during the fitting of the partial charges to the MEP of individual conformations as implemented in NWCHEM.[36] The calculations of the AM1-BCC charges were carried out using Antechamber, a module of AmberTools 1.4,[29] and they were averaged over 1000 representative structures.

In each of these systems, we have used two kinds of water models, TIP3P[37] and SPC/E,[38] to solvate the triad in the bulk system and in various sizes of confinement using the modules from Visual Molecular Dynamics (VMD).[39]

II.2. Simulation Preparation. *Periodic Boundary Conditions (PBC).* PBCs were implemented in a cubic box of water molecules (10 nm ×10 nm ×10 nm) prepared by VMD.[39] The energy of this bulk solvent system was first minimized using a conjugate gradient method and then equilibrated in four steps by using NAMD[40] as follows: (1) gradually heat up water molecules to 300 K while keeping triad fixed in space; (2) gradually heat up the system to 300 K with a temperature step of 3 K and run a 2-ps simulation per temperature step under constant NVT conditions using Langevin dynamics; (3) equilibrate the system at 300 K and 1 atm under constant NPT conditions using Nosé−Hoover Langevin piston pressure control[41,42] to adjust the water density to 0.97 g/cm^3; (4) equilibrate the system at 300 K under constant NVT conditions for 200 ps. Finally, 20 randomly selected configurations were chosen, and each was individually equilibrated at several other temperatures to be used as the input for the REMD simulations (see section II.4).

Spherocylindrical Boundary Conditions (SCBC). The triad was solvated in three nanosizes of SC by VMD[39] in Table 1.

dx.doi.org/10.1021/jp212273n | J. Phys. Chem. B 2012, 116, 8460−8473

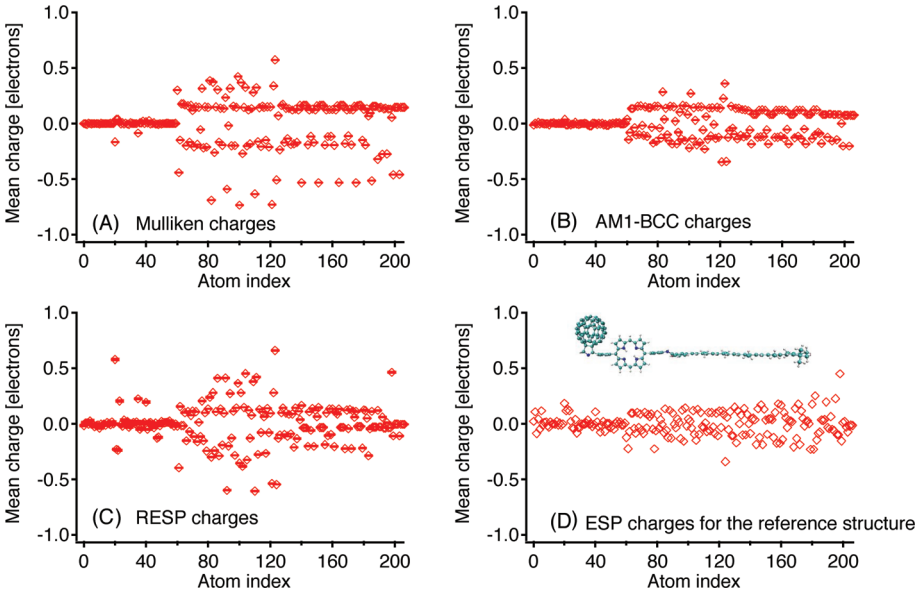

Figure 2. Atomic charges along atomic indices averaged over 1000 structures selected from MD simulations (see Methods Section). The charges were calculated by (A) using Mulliken population analysis, (B) AM1-BCC method, and (C) fitting to an MEP (RESP) method. The atomic charges in panel D were calculated by fitting to the electrostatic potential of the reference structure.[25]

Table 1. The Number of Water Molecules and the Water Density for a Given Simulation System

system	size	water density (g/cm^3)	no. of water molecules	no. of replicas
periodic cubic box (PBC)	9.9 nm × 9.9 nm × 9.9 nm	0.97	31809	60
spherocylinder (SC9.5)	*a*: 3.65 nm; *b*: 2.21 nm	1.02	5338	40
spherocylinder (SC6.5)	*a*: 3.65 nm; *b*: 1.91 nm	1.02	3850	40
spherocylinder (SC3.5)	*a*: 3.65 nm; *b*: 1.61 nm	1.02	2618	32

These sizes were defined by the following procedure: First, an extended form of the triad was solvated in the smallest SC, and then thick layers of one (SC3.5), two (SC6.5), and three (SC9.5) water models were padded, respectively. The spherocylinder was defined by two parameters, the half-length of the cylinder, *a*, and the radius of the hemisphere, *b*, in Figure 1C. The confining energy of an atom under SCBC is defined as follows:

1 If an atom is within the hemisphere region, then the confining energy is $E = k(r_h - b)^2$, when $r_h \geq b$. Here, r_h is the distance between an atom to the origin of the left or right hemisphere, and k is 10 kcal/mol/Å^2.
2 If an atom is within the cylindrical region, then $E = k(\rho - b)^2$, when $\rho \geq b$. Here, ρ is the distance from the atom to the central axis of the cylinder, and k is 10 kcal/mol/Å^2.

Each of the confinement systems underwent energy minimization by a conjugate gradient method, followed by these equilibration steps: (1) gradually heat up water molecules to 300 K while keeping the triad fixed in space; (2) gradually heat up the system to 300 K with a temperature step of 3 K and run a 2-ps simulation per temperature step under constant NVT conditions using Langevin dynamics; (3) equilibrate the system at 300 K under constant NVT conditions for 200 ps. Then 20 randomly selected configurations were chosen, and each was individually equilibrated at several other temperatures to be used as the input for the REMD simulations (see section II.4).

II.3. MD Simulations. Simulations were executed using the NAMD[40] package in order to investigate the thermodynamic properties of the triad in a bulk solvent system and in various nanosizes of SC (Table 1). The SHAKE[43] algorithm was employed to keep a fixed bond length in all bonds, and the integration time step is 2 fs. The damping coefficient for the Langevin dynamics is 5 ps^{-1}. For the bulk system, the switching distance for van der Waals force was set at 10 Å, and the cutoff was set at 12 Å. The electrostatics interactions were calculated using the particle mesh Ewald (PME)[44] method. For the confinements, the switch for the van der Waals force was applied at 140 Å, and the cutoff for both the van der Waals interaction and the electrostatics interaction was set at 150 Å, far beyond the size of the largest confinement in this study. The data points were collected at every 1 ps, which is greater than the correlation time.

II.4. REMD. The replica exchange method[28,31] was used to enhance the sampling efficiency by incorporating multiple copies (replicas) of MD simulation over a broad range of temperatures. An exchange between two neighboring replicas *i* and *j* is accepted with a probability

$$P_{acc} = \min\{1, \exp[(\beta_i - \beta_j)\cdot(E_i - E_j)]\} \quad (1)$$

where $\beta = 1/k_B T$, and E_i represents the potential energy of the *i*th system. For each system, the number of replicas are determined to obtain an optimal distribution of target temperatures, generated as geometric series, between 280 and 400 K for an overall exchange rate of 20−30%, which is suitable for REMD. The exchange interval is 4 ps. The number of replicas for the bulk solvent and confinement systems is shown in Table 1. The configurations from the replicas were collected every 1 ps. The weighted histogram analysis method (WHAM)[45] was employed to compute the free energy and thermodynamic averages. For the PBC, each of the 60 replicas is simulated for 30 ns, and for the SCBC, each of the 32 replicas (SC3.5) or 40 replicas (SC6.5 and SC9.5) is simulated for 20 ns.

dx.doi.org/10.1021/jp212273n | J. Phys. Chem. B 2012, 116, 8460−8473

II.5. Characterization of the Water Structure. *Water Density Profile.* The water density profile surrounding the center of mass (COM) of each component of the triad was computed as a function of the radial distance, *r*, from the COM, to the oxygen atom of a water molecule. The number of water molecules was computed in a spherical shell of thickness Δ = 0.1 Å centered at the COM with a radius *r*. This number was normalized by the volume of the shell inside a nanosized SC. The intersection volume of an infinity cylinder and a sphere is computed using the analytical equation,[46] and the intersection volume of a sphere and a hemisphere is computed using the Monte Carlo method.

Water Orientation. The orientation of a water molecule surrounding the COM of each component of the triad is defined by the cosine of the angle (θ) between the vectors of COM-O and O−H bonds[26] where COM-O is a vector pointing from the COM of each component of the triad to the water oxygen atom.

III. RESULTS

III.1. Ensemble Averaged Charge Assignment on the Triad. The three sets of thermally averaged point charges obtained using the Mulliken population analysis, the AM1-BCC, and the RESP charges models are plotted in Figure 2A,B,C, respectively. In general, the agreement between all of the three methods is satisfactory with regard to the lowest absolute values of the charges obtained by the AM1-BCC method (Figure 2B). However, there are several noticeable differences between the charges calculated with these three methods. For example, in Figure 2A, the Mulliken charges of the methyl carbons located on the carotenoid, such as C140, C151, C164, and C175, are −0.58 *e* compared to the ones obtained from the AM1-BCC methods in Figure 2B and the RESP in Figure 2C, which are about 0.10−0.20 *e* and −0.20 *e*, respectively. Similarly, the Mulliken charges on the two pyrrole nitrogens of porphyrin N82 and N100, −0.69 and −0.73 *e*, respectively, are substantially higher than the corresponding charges calculated with the RESP (N82 and N100, −0.30 *e*) and the AM1−BCC (N82, −0.13 *e*; N100, −0.22 *e*) methods.

We have observed a large fluctuation of the RESP charges (Figure 2C) on the fullerene carbon atoms that are in the order of 1 *e*. We have taken a sufficient amount of structures (i.e., 1000) for each method so that the error of the mean (standard deviation divided by the square root of mean) is small. The averaged RESP charges of C_{60} carbons are close to zero, except the two atoms that are shared with the hinged pyrrole group. These carbon atoms with large partial charges experience a much smaller variation less than 0.10 *e* when they were calculated using Mulliken or AM1-BCC methods. The ESP charges of the C_{60} carbons computed by Baruah's group have unphysical large values for a ground state (Figure 2D). These charges were obtained for the single geometry DFT optimized fully extended structure of a triad, which cannot reflect the effects of thermal fluctuations on the atomic charges. Consequently, we have decided to use the set of thermally averaged AM1-BCC charges for the ground-state triad in Figure 2B in our simulations. Further discussions on using the charges from the AM1-BCC calculation instead of Mulliken calculation for our MD simulations are provided in the Discussion Section IV.1.

III.2. Favorable Positions of Each Component of the Triad in the SC. To investigate the impact of confinement on the triad, as a first step we determined the favorable positions of the triad in several sizes of the SC at 350 K. The free energy as a function of the position of the COM of each component of the triad, *r*, is shown for the confinement of SC9.5 (red curve), SC6.5 (green curve), and SC3.5 (blue curve) in Figure 3. If the COM of each component of the triad is in the cylindrical region, *r* is in a normal direction radially away from the principal axis of the cylinder. If the COM of each component of the triad is in the two hemispherical regions, *r* is radially away from the origin of the left or the right hemisphere. Parts A and D, B and E, and C and F of Figure 3 are for the C_{60}, porphyrin, and carotenoid, respectively. We have also investigated the impact of two types of water models, TIP3P and SPC/E, by solvating the triad systems in Figure 3A,B,C, for the former, and in Figure 3D,E,F for the latter.

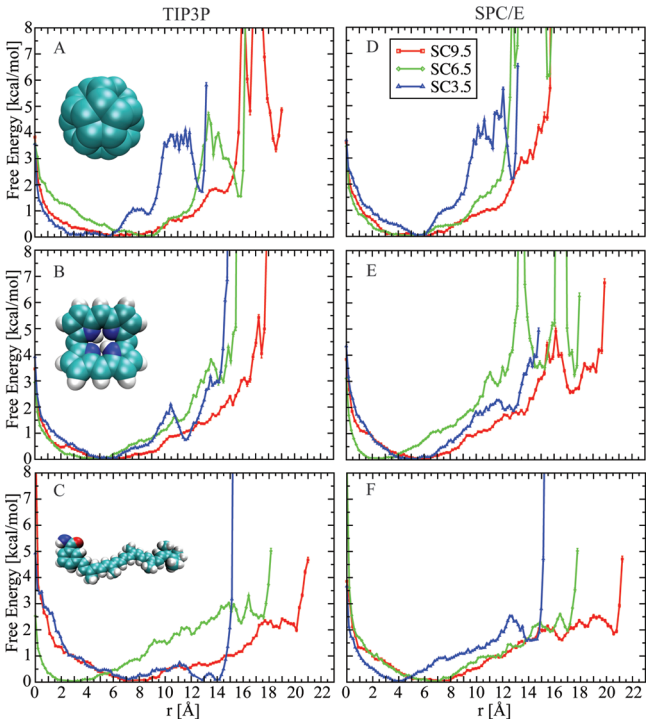

Figure 3. The free energy as a function of the position, *r*, relative to the central axis of the sphercocylinder. If the COM of each component of the triad is in the cylindrical region, *r* is in a normal direction radially away from the principal axis of the cylinder. If the COM of each component of the triad is in the two hemispherical regions, *r* is radially away from the origin of the left or the right hemisphere. The free energy of each component of the triad—(A,D) C_{60}, (B,E) porphyrin, and (C,F) carotenoid—is plotted in the panels. Each panel includes the conditions of several sizes of the confinement: SC9.5 in red, SC6.5 in green, and SC3.5 in blue. These systems were solvated by two types of water models: TIP3P in A, B, and C and SPC/E in D, E, and F. Error bars are included.

Figure 3A shows that the position of the free energy minimum of the C_{60} solvated by TIP3P water is located close to the interior of a confinement. The minima of free energy is around *r* = 5.5 Å for SC9.5 (red curve), *r* = 8.3 Å for SC6.5 (green curve), and *r* from 3 to 6 Å for SC3.5 (blue curve). Note that there are other local minima close to the surface, and they are shallower than the ones in the interior by 2−3 kcal/mol: *r* = 18.5 Å for SC9.5, *r* = 15.7 Å for SC6.5, and *r* = 12.9 Å for SC3.5. When the size of the confinement decreases, the free energy difference between the interior and the surface narrows from 3.4 kcal/mol (SC9.5) to less than 2 kcal/mol (SC3.5), indicating that there is a much greater probability of finding the C_{60} on the surface in smaller size of confinement.

dx.doi.org/10.1021/jp212273n | J. Phys. Chem. B 2012, 116, 8460−8473

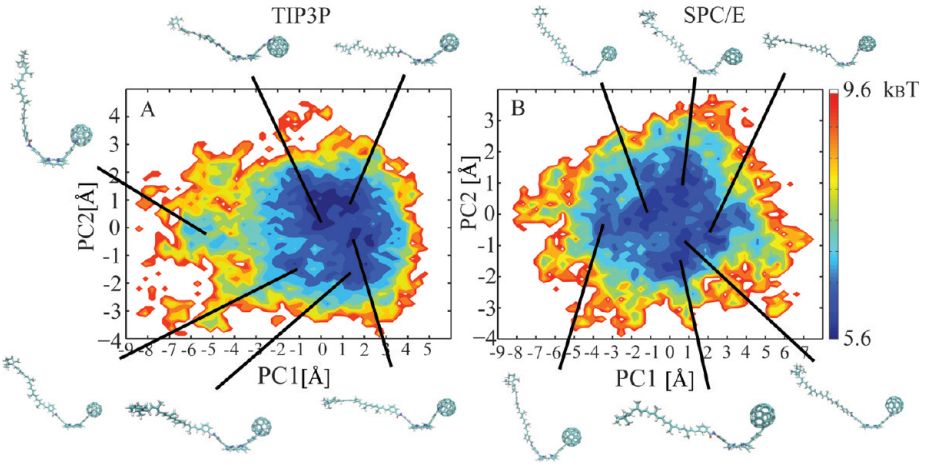

Figure 4. 2-D free energy as a function of the first principal component (PC1) and the second principal component (PC2) for the triad in the bulk system solvated by either (A) TIP3P water or (B) SPC/E water. The color scale is given in units of k_BT, where k_B is the Boltzmann constant and T is temperature at 350 K. Six representative structures of the triad are illustrated in each panel.

Figure 3D shows that the position of the free energy minima of the C_{60} is also at r = 6 Å for several sizes of the confinement when the triad is solvated by SPC/E water, representing that the C_{60} is likely to stay in the interior of the confinement. In contrast to the system solvated by TIP3P water, the local second minima near the surface for SC9.5 (red curve) and SC6.5 (green curve) are much weaker. However, there is a local minimum at r = 13 Å for SC3.5 (blue curve), which is the same position for SC3.5 in TIP3P water in Figure 3A. The free energy at the second free energy minima (r = 13 Å) for SC3.5 for SPC/E water (2.2 kcal/mol) is higher than that for TIP3P water (1.7 kcal/mol), suggesting that the former has less population of C_{60} residing at the surface than the latter.

For porphyrin, the minima of free energy are close to the interior of a confinement for both TIP3P and SPC/E water in Figure 3B,E, respectively. In Figure 3B (TIP3P), the position of the free energy minima is r = 5.1 Å for SC9.5, r = 4.2 Å for SC6.5, and r = 5.6 Å for SC3.5. In the smallest confinement, SC3.5, a second local minimum exists near the surface. The free energy difference between the two minima at the interior and at the surface is approximately 0.8 kcal/mol. The probability of porphyrin to be at the surface increases when the size of the confinement decreases. However, this trend has not been strong for the porphyrin solvated by SPC/E water in Figure 3E, where the position of the free energy minima ranges from r = 2.5 Å to r = 5.5 Å, which is close to the interior of the confinement.

In Figure 3C, the free energy minima for the COM of the carotenoid solvated by TIP3P water are close to the interior of the confinement for SC9.5 (red curve) and SC6.5 (green curve), where r is broadly distributed around r = 3−8 Å, respectively. This broad distribution is accounted for by the large structural flexibility in the carotenoid. When the size of the confinement reduces (SC3.5), a second minimum at r = 14 Å that is close to the surface emerges. The free energy difference between the carotenoid being at the interior and near the surface is nearly 0, indicating that there is about the same population of carotenoid at both locations. By contrast, the positions of the free energy minima for the triad solvated by SPC/E water are r = 7, 6, and 4 Å for SC9.5, SC6.5, and SC3.5, respectively, in Figure 3F, showing that the carotenoid is likely to stay in the interior of the confinement.

We have further broken down 40 atoms in the carotenoid into eight classes based on their profiles of water density in Table S2 (Supporting Information). The free energy as a function of position of a representative of each class is shown in Figure S1. We found that the carbon index 199, at the end of the carotenoid, is likely to stay at the surface in the confinement, which is similar to the methane in the confinement.[47]

III.3. 2-D Free Energy Landscape of the Triad. Under thermal fluctuations, the triad bends and twists around the hinges of the two phenyl groups and around the carotenoid. We have applied the PCA approach on the triad in the bulk systems in order to characterize its structural variance at T = 350 K. The 2-D free energy profiles as a function of the first two principal components (PC1 and PC2) for the triad solvated by either TIP3P water or SPC/E water are provided in Figure 4A,B, respectively. Several representative structures at the basins of the free energy have been illustrated in each panel, and they are far from a fully extended structure, as the one optimized by the DFT.[9] Differences between Figure 4A and B indicate that the distribution of the triad conformation is broad, and the free energy barrier between local minima is less than 1 k_BT. Small differences in solvent models can easily modulate the population of the triad at ambient conditions.

To further characterize the structures of the triad under effects of confinement, several 2-D free energy landscapes were plotted as a function of the end-to-end distance (d) and the shape parameter (S) of the triad for the bulk system (Figure 5A,E) and for three sizes of SC: SC9.5 (Figure 5B,F), SC6.5 (Figure 5C,G) and SC3.5 (Figure 5D,H). d is defined as the distance measured from the carbon atom index 20 on the C_{60} to the carbon atom index 192 on the carotenoid (Figure 5I). S, derived from an inertia tensor[48] (see Supporting Information), ranges from −0.25 to 2.00, where S = −0.25 represents an oblate spheroid (e.g., disk) and S = 2.00 represents a prolate spheroid (e.g., rugby ball). The shape parameter of a sphere is S = 0. These free energy diagrams were calculated for both water models, TIP3P (Figure 5A,B,C,D) and SPC/E (Figure 5E,F,G,H), to investigate the impact of solvation on the triad. The ensemble of structures was divided into a small number of clusters by using a clustering method based on a neural-net algorithm.[49] The structural characteristics of the two most

dx.doi.org/10.1021/jp212273n | J. Phys. Chem. B 2012, 116, 8460−8473

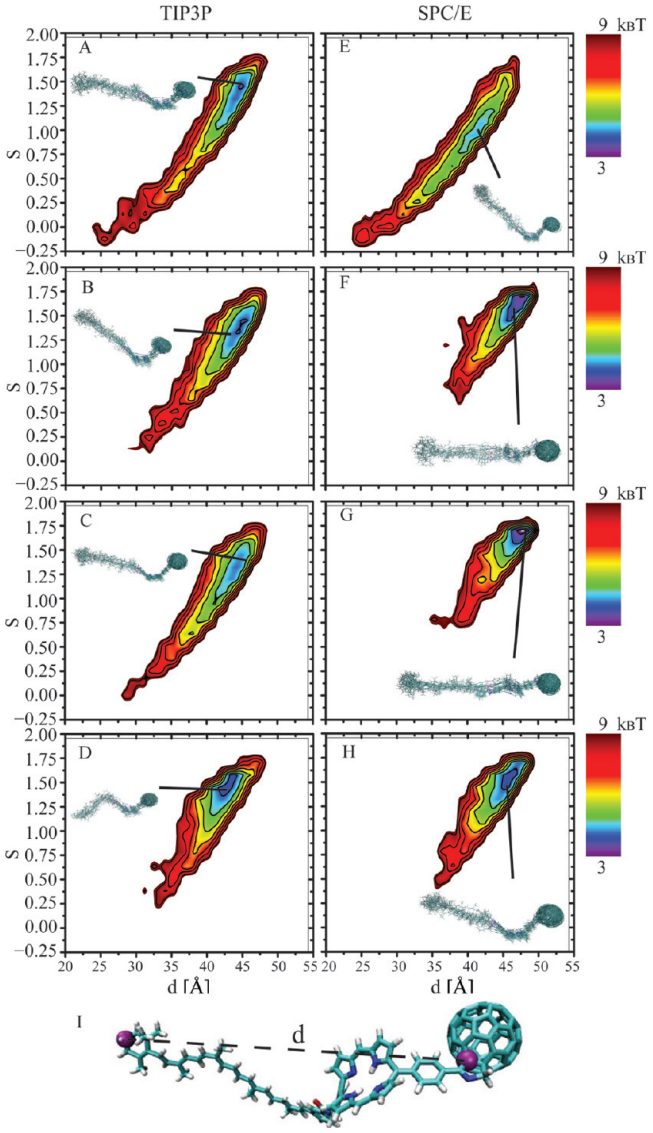

Figure 5. 2D-free energy as a function of the end-to-end distance, *d*, and the shape parameter, *S*, of the triad. The solvated triad was in the bulk system (A,E) and in three sizes of nanospherocylindrical confinement: B and F for SC9.5; C and G for SC6.5; and D and H for SC3.5. The triad was solvated by two types of water models: TIP3P in the left column (A–D) and SPC/E (E–H) in the right column. The color bar is scaled in units of k_BT. *d* is defined as the distance measured from the carbon atom index 2 on the C_{60} to the carbon atom index 192 on the carotenoid. Both atoms were labeled in purple spheres in panel I for visual guidance.

dominant clusters are shown in Table 2 in order to further facilitate the structural analysis on the triad in the next paragraph.

When comparing the 2-D free energy landscape of the triad in the bulk systems solvated by TIP3P water (Figure 5A) with the one solvated by SPC/E water (Figure 5E), the end-to-end distance, *d*, for the free energy minimum of the latter is reduced by 3 Å, and *S* is reduced by 50%. When we further analyzed the structural differences in the dominant structures in Table 2, *d* is 41.85 Å and *S* is 1.04 for the triad solvated by SPC/E water compared to *d* = 45.67 Å and *S* = 1.47 in TIP3P water. We have also computed the orientation of the phenyl group, porphyrin, and the second phenyl group by defining a pseudodihedral angle Φ composed of four atoms illustrated in Figure 1B. Φ is around 0° for both dominant structures. Both of them are structurally compact as a result of a "boat" shaped complex (_/) with the two phenyl groups flickered inward at the same side of the porphyrin.

These solvent-dependent structural differences become more pronounced when SC conditions are imposed on the triad. Further, the differences in the triad ensemble structures between the two water models grow greater as the size of the confinement reduces. First, the confinement effect was analyzed for TIP3P water in Figure 5A,B,C,D with respect to the bulk (PBC), SC9.5 (largest confinement), SC6.5, and SC3.5 (smallest confinement). From Table 2, the percentage of the dominant structure in an ensemble under the bulk condition is 26% with an average *d* of 45.67 Å, while the dominant structure for SC9.5 increases to 37% with *d* of 43.43 Å. As we reduce the size of the confinement, a second type of dominant structure with a new "kink" in the middle of the carotenoid emerges. An illustration of this structure is provided in Figure 5D and its end-to-end distance is around 42 Å. This structure dominates in the second major cluster for SC6.5 and forms in the largest cluster for SC3.5. The reason for the appearance of this kink is because the affinity of carotenoid to the surface localization increases when the size of confinement reduces in the system for the TIP3P water model. Indeed, Figure S1O shows that a single free energy minimum for of the carbon atom of index 199 (at the end of the carotenoid) is located near the surface at *r* = 15 Å in a confinement of SC3.5.

On the other hand, for the SPC/E water systems, we found that the triad at the global minimum prefers a rather extended and rod-like structure in the confinement conditions (Figure 5F,G,H for SC9.5, SC6.5, and SC3.5, respectively) compared to the bulk system (Figure 5E). *d* increases by 3 Å, and *S* increases by 50% in the confinement compared to the bulk. Interestingly, in Table 2, *d* of all of the three dominant clusters for SC9.5, SC6.5, and SC3.5 solvated by SPC/E water exceed 46 Å. It is found that the pseudodihedral angle Φ equals −103° for the structure with *d* = 46.6 Å, and Φ equals −135° for the structure with *d* = 48.4 Å. The former constitutes a "chair"-shaped complex (/\/) that accounts for a rather extended structure with respect to the boat-shaped complex (_/) populated in the bulk conditions. A representative chair structure is provided in Figure 5F. The latter (Φ = −135° and *d* = 48.4 Å) forms a nearly flat complex (____) with the three aromatic compounds that resemble the fully extended structure with *d* = 49.4 Å in Baruah's study. A representative "flat" structure is given in Figure 5G. This fully extended structure with *d* = 48.4 Å appears in the second dominant cluster for SC9.5 and becomes the first dominant cluster for SC6.5. When solvated by SPC/E water, the most favorable positions for triad is still at the interior of the confinement for SC9.5 and SC6.5; the confinement has a stronger effect over hydration interactions. However, when the confinement is further reduced to SC3.5, the possibility of being populated at the surface increases for some of the carotenoid atoms (e.g., Figure S1O) and that decimates the population of the extended structures with *d* = 48.4 Å. As a result, the boat-like compact structures with *d* = 45 Å and Φ ∼ 0° dominate in the first and second clusters.

III.4. Radial Distribution of Water Density Surrounding Each Component of the Triad. The profiles of the distribution of water density (ρ_{water}) as a function of the radial distance from the COM of each component of the triad are shown in Figure 6. ρ_{water} for C_{60}, porphyrin, and carotenoid are plotted in Figure 6A,D, B,E, and C,F, respectively. The results

dx.doi.org/10.1021/jp212273n | J. Phys. Chem. B 2012, 116, 8460–8473

Table 2. Structural Characteristics and Percentage of the Triad Conformations for the First Two Dominant Clusters in the Bulk System (PBC) and Various Sizes of Confinement (SC9.5, SC6.5, and SC3.5) Solvated by Either the TIP3P or the SPC/E Water Model[a]

			Percentage (%)	d (Å)	S	Φ (deg)
TIP3P	Cluster 1	PBC	26.56	45.67 ± 0.01	1.47 ± 0.00	3.80 ± 0.14
		SC9.5	37.01	43.43 ± 0.01	1.26 ± 0.00	−2.73 ± 0.11
		SC6.5	33.46	45.40 ± 0.01	1.40 ± 0.00	−4.46 ± 0.14
		SC3.5	29.50	42.46 ± 0.01	1.41 ± 0.00	−2.91 ± 0.15
	Cluster 2	PBC	22.77	43.26 ± 0.01	1.20 ± 0.00	3.22 ± 0.14
		SC9.5	34.91	45.84 ± 0.01	1.46 ± 0.00	−3.88 ± 0.12
		SC6.5	20.85	42.19 ± 0.02	1.08 ± 0.00	−2.34 ± 0.15
		SC3.5	22.82	44.06 ± 0.01	1.51 ± 0.00	−3.27 ± 0.33
SPC/E	Cluster 1	PBC	26.46	41.85 ± 0.01	1.04 ± 0.00	−3.75 ± 0.13
		SC9.5	35.10	46.60 ± 0.01	1.57 ± 0.00	−102.82 ± 0.96
		SC6.5	41.72	48.43 ± 0.01	1.70 ± 0.00	−134.59 ± 0.76
		SC3.5	27.17	47.37 ± 0.01	1.63 ± 0.00	−2.91 ± 0.15
	Cluster 2	PBC	20.35	44.78 ± 0.02	1.33 ± 0.00	−3.09 ± 0.15
		SC9.5	34.87	48.18 ± 0.01	1.66 ± 0.00	−124.18 ± 0.89
		SC6.5	35.65	46.76 ± 0.01	1.61 ± 0.00	−111.62 ± 1.00
		SC3.5	24.61	45.36 ± 0.01	1.43 ± 0.00	−3.27 ± 0.33

[a] d is the end-to-end distance defined in the text and shown in Figure 5I. S is the shape parameter. Φ is the pseudodihedral angle defined by four atoms, whose indices are 60, 75, 93, and 121, respectively, and is shown in Figure 1B.

for TIP3P water systems are shown in the panel of Figure 6A,B,C, and those for SPC/E are shown in the panels of Figure 6D,E,F.

C_{60}. In Figure 6A (TIP3P) and D (SPC/E), the position of the first peak for C60 (6.6 Å) is measured from its COM, and the distance between the two is approximately equal to the sum of the size of a water in the first hydration shell for a methane (~3.5 Å[50]) and the radius of the C_{60} (3.5 Å). The amplitude of the first peak for the C_{60} increases by 11% by the confinement (SC3.5) in TIP3P water in Figure 6A. Under confinement, the valley of the first water-mediated contact minimum at r = 8.1 Å is lower, while the amplitude of the second hydration shell at r = 9.4 Å is greater than those in the bulk system. In Figure 6D for the SPC/E water model, it is shown that ρ_{water} profiles are very similar to those for the TIP3P water model. The amplitude of the first peak for the C_{60} increases by 12% by the confinement (SC3.5) in SPC/E water in Figure 6D. It is suggested that under confinement, water molecules are very structured around C_{60}, and its impact can be felt within two hydration layers.

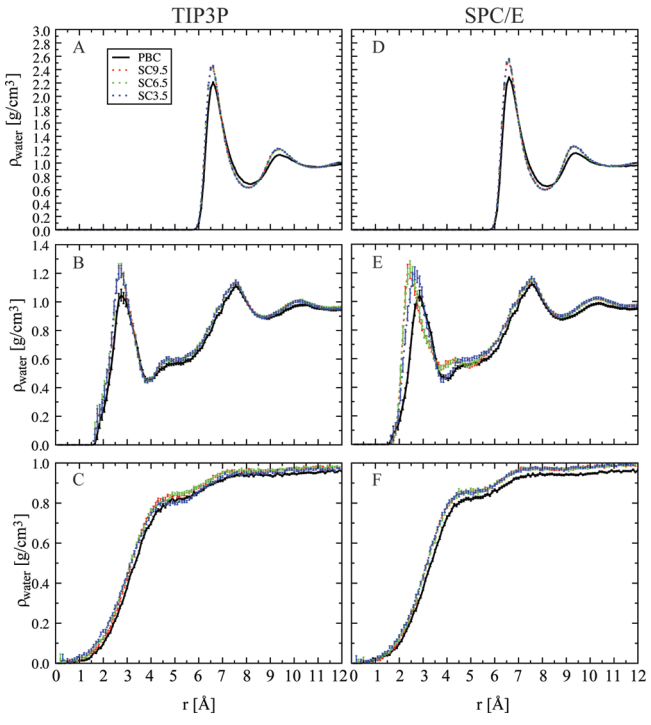

Figure 6. The density of water molecules, ρ_{water}, as a function of distance, r, with respect to the COM of C_{60} in A and D, and porphyrin in B and E, and carotenoid in C and F. Each simulation system including the triad is solvated by either the TIP3P water model (A,B,C) or the SPC/E water model (D,E,F). Each panel includes the conditions of a bulk system under a PBC and several sizes of the SC: PBC, black; SC9.5, red; SC6.5, green; and SC3.5, blue. Error bars are included in the profiles.

Porphyrin. In Figure 6B (TIP3P) and E (SPC/E), ρ_{water} is measured from the COM of porphyrin that resembles a square box. The water density profiles of the porphyrin are more complicated than the C_{60} because the porphyrin is not a sphere. The second peak appears at r = 7.55 Å, and the separation between the first peak and the second peak represents half the diagonal of the porphyrin (4.8 Å). In Figure 6B (TIP3P), the amplitude of the first peak at r = 2.75 Å increases by 4% in the presence of confinement (SC3.5), and all of the water density profiles for SC9.5, SC6.5, and SC3.5 overlap each other. There is little difference in ρ_{water} at a distance greater than the first hydration shell. However, in Figure 6E (SPC/E), it is shown that the positions of the first peak shift toward the right when the size of the confinement decreases. In addition, the valley between the first and second peaks under confinement becomes shallower than that in the bulk, indicating that porphyrin is better solvated under confinement.

Carotenoid. In Figure 6C (TIP3P) and F (SPC/E), ρ_{water} is measured from the COM of the carotenoid that is structurally malleable. In Figure 6C, profiles of ρ_{water} for the bulk system (black curve) and for various sizes of the confinement (red, green, and blue curves) nearly overlap each other. There is no peak for the first hydration shell with ρ_{water} greater than 1. From

dx.doi.org/10.1021/jp212273n | J. Phys. Chem. B 2012, 116, 8460−8473

r = 4 to 7 Å, ρ_{water}, averaged over the COM, is less than 1. We have further broken down the patterns of ρ_{water} for the 40 atoms on the carotenoid into eight classes (Table S2) by the differences in the position of the first peak, the height of the peak, and the number of the peaks. A representative ρ_{water} of each class is shown in Figure S2. The density profiles of water molecules of these eight representatives, whose indices are 125, 126, 135, 137, 139, 140, 172, and 199, are shown in Figure S2A–H, respectively. In Figure S2I, the carotenoid is colored by the eight classes. ρ_{water} of the carbon atom with an index of 140, which is a methyl group, is similar to that of methane (Figure S2F). The position of the first peak of water density profile of the carbon atom with an index of 139 (Figure S2E), which is the carbon atom immediately bonded to the methyl group, shifts to the right at r = 4.7 Å as a result of volume exclusion from the methyl group. Other heavy atoms (Figure S2A,B,C,D,G,H) along the main chain of the carotenoid have less access to water molecules, and their ρ_{water} is below 1 at r < 7 Å.

Phenyl Groups. The water density profiles of the first phenyl group (between the C_{60} and porphyrin) and the second phenyl group (between the porphyrin and carotenoid) are shown in Figure S3A,C, and Figure S3B,D, respectively. In Figure S3A, the first hydration peak is less than 1, indicating that the phenyl group has less access to water molecules. The amplitude of the first peak increases by 3% when the confinement (SC9.5) is considered for TIP3P water. In Figure S3C for SPC/E water, the water density profile is similar to that for TIP3P water. The amplitude of the first peak for SPC/E is 5% greater than that for TIP3P in all confinement conditions. In Figure S3B,D, it is shown that the water density profiles of the second phenyl group are very similar to those of the first phenyl group. Noticeably, the amplitude of the first peak for the second phenyl group is 12% greater than the first phenyl group in all confinement for TIP3P water. A similar trend is observed for SPC/E water, in that the first peak of the second phenyl group is 9% greater than that of the first phenyl group in overall confinement. It is because the C_{60} close to the first phenyl group prevents it from accessing the water molecules.

III.5. Water Orientation Surrounding the Triad in SC. Figure 7 shows the probability distribution of $\cos(\theta)$ of water molecules within 8 Å of the COM of the C_{60} (Figure 7A,D), porphyrin (Figure 7B,E), and carotenoid (Figure 7C,F). θ is defined in the Methods Section. For C_{60} in Figure 7A,D, the two major peaks at $\cos(\theta)$ = −0.33 and 1 (θ = 109° and 0°), showing that the water molecules self-assemble into clathrate-like structures (Figure 7G) in the proximity of the C_{60}. For TIP3P water (Figure 7A), the amplitude of the peak at $\cos(\theta)$ = −0.33 in the overall confinement (0.82) is slightly higher than that in the bulk system (0.80), which means that the structure of water molecules is more ordered in the confinement. For SPC/E water (Figure 7D), the height of the peak at $\cos(\theta)$ = −0.33 in the overall confinement (0.92) is higher than that in the bulk system (0.88). The amplitude of the peaks at $\cos(\theta)$ = −0.33 and 1 in a bulk system solvated by SPC/E water (0.88) is higher than that solvated by TIP3P water (0.80). Likewise, the valleys at $\cos(\theta)$ = −1 and 0.50 of the system solvated by TIP3P water is lower than those by SPC/E water. Both observations point to the fact that the structure of SPC/E water surrounding C_{60} is more ordered than TIP3P water.

Figure 7B,E corresponds to the probability distribution of $\cos(\theta)$ of water molecules within 8 Å of the COM of the porphyrin. It is noted that the overall distribution is flat, and the probability is around 0.5, close to a uniform distribution. Profiles of $\rho(\cos(\theta))$ for the bulk and confinement systems overlap with each other, regardless of the type of the water model, indicating that porphyrin is less susceptible to solvation. Still, there is a round peak close to $\cos(\theta)$ = 0, corresponding to water molecules that are perpendicular (θ = 90°) to the solute, and the oxygen is facing close to the solute (Figure 7G). This preferred orientation of water molecules is a better hydrogen bond (HB) acceptor to the hydrogen atoms attached to the nitrogen atoms at the center of the porphyrin. This result is similar to that obtained by Levitt[51] when the spatial distribution of water orientation was analyzed surrounding a benzene.

Figure 7C,F corresponds to the probability distribution of $\cos(\theta)$ of water molecules within 8 Å of the COM of the carotenoid. Profiles of $\rho(\cos(\theta))$ for the bulk and confinement systems overlap with each other, and they are quite flat, regardless of the type of the water model. Its distribution curves still generally follow the hills and the valleys of those of C_{60}, but in much less distinction. It is suggested that carotenoid is also less susceptible to solvation.

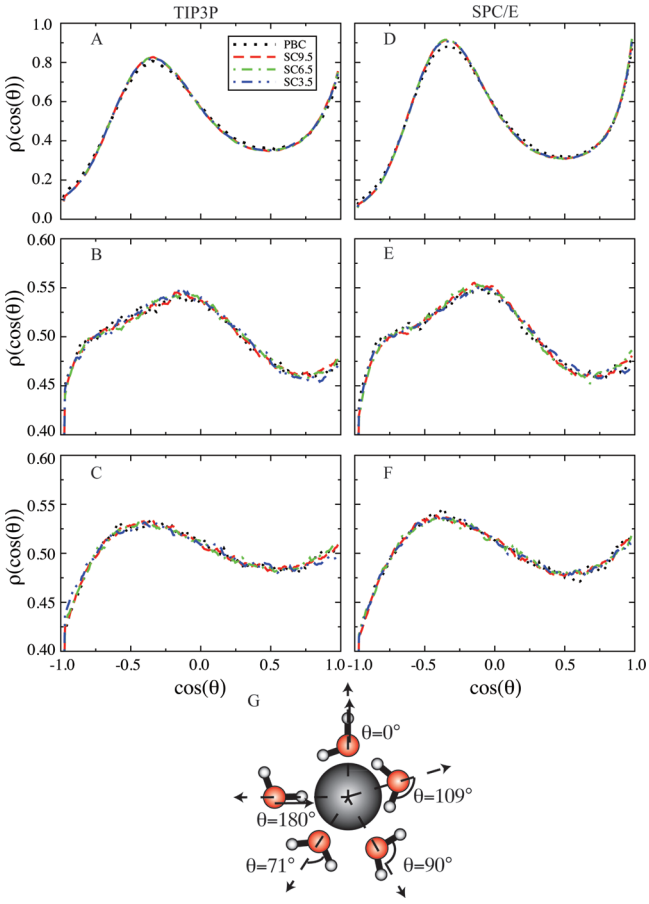

Figure 7. Probability distribution of the water orientation within 8 Å measured from the COM of each component of the triad: (A,D) C_{60}, (B,E) porphyrin, and (C,F) carotenoid. Each panel includes the conditions of a bulk system under PBC and several sizes of the SC: PBC, black; SC9.5, red; SC6.5, green; and SC3.5, blue. In addition, these systems were solvated by two types of water models: TIP3P in A, B, and C, and SPC/E in D, E, and F. (G) This schematic diagram shows the typical organizations of two water molecules surrounding a hydrophobic solute in a clathrate-like structure and two in an inverted structure, respectively. The two most probable orientations of the angle θ (0 and 109°) are shown on this diagram. The two inverted structures, θ = 71° and 180°, are shown on this diagram as well.

dx.doi.org/10.1021/jp212273n | J. Phys. Chem. B 2012, 116, 8460–8473

III.6. 2-D Water Orientation Distribution Surrounding the C_{60} of the Triad. Motivated by Figure 7 where there are large distinction in water orientation around the C_{60}, we investigated the 2-D probability distribution as a function of water orientation ($\cos(\theta)$) and the radial distance away from the COM of C_{60} in Figure 8A for TIP3P water and in Figure 8E for SPC/E water. The differences in the probability distribution between the bulk system (Figure 8A,E) and various sizes of confinement are shown in Figure 8B,F for SC9.5, Figure 8C,G for SC6.5, and Figure 8D,H for SC3.5.

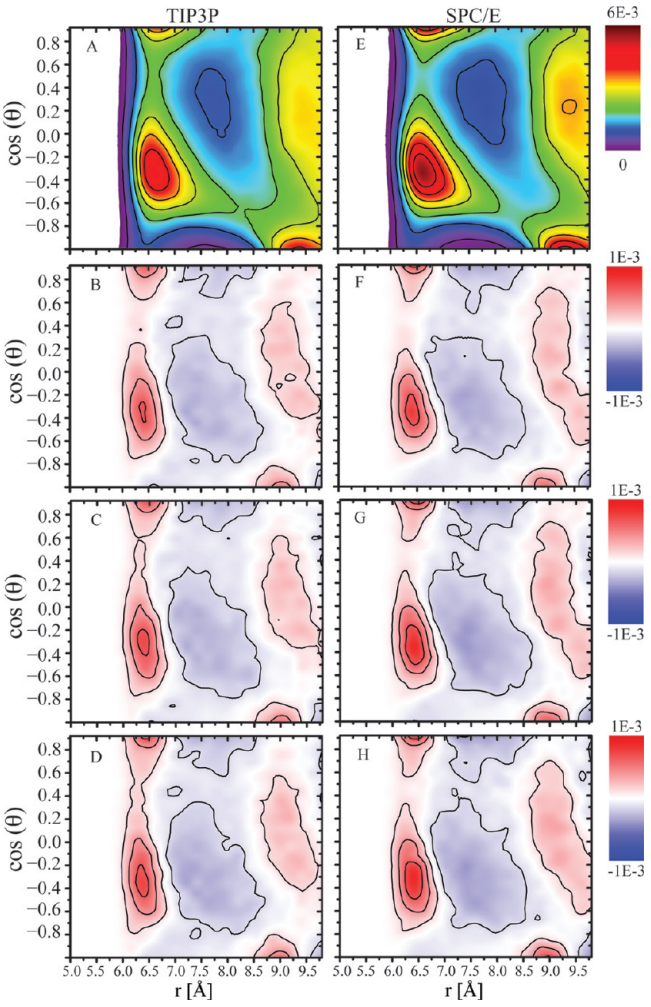

Figure 8. (A,E) Probability distribution of the distance, r, between O in the proximal water molecules and the COM of C60 and their corresponding angular orientation between O−H and COM-O in terms of $\cos(\theta)$ in bulk systems. (B and F, C and G, D and H) The difference in the probability distribution between the bulk system and that in the SC is plotted for SC9.5, SC6.5, and SC3.5, respectively, using the same x- and y-axes. In addition, the systems are solvated in two water models: TIP3P, left column, and SPC/E, right column.

In Figure 8A,E, there are four maxima. Two appear at r = 6.5 Å, $\cos(\theta) = 1$ and r = 6.5 Å, $\cos(\theta) = -0.33$, indicating that the water molecules favor clathrate-like structures (Figure 7G) in the first hydration shell. The other two appear at r = 9.5 Å, $\cos(\theta) = 0.33$ and r = 9.5 Å, $\cos(\theta) = -1$, corresponding to inverted clathrate-like structures (Figure 7G) in the second hydration shell. For SPC/E water, the probability at r = 6.5 Å and $cos(\theta) = -0.33$ in Figure 8E is higher than for TIP3P water in the bulk systems in Figure 8A, whereas the probability between the two hydration shells for SPC/E water are lower than for TIP3P water. It is suggested that SPC/E water molecules are more ordered than the TIP3P water model because SPC/E's HOH angle is modeled after a perfect tetrahedron, so it packs better in space.

Regarding the confinement effect, the difference probability profiles (Figure 8B,C,D) show the emergence of several red areas peaked at r = 6.5 Å, $\cos(\theta) = 1$ and r = 6.5 Å, $cos(\theta) = -0.33$, representing an increase in the probability of the water molecules with clathrate-like structures in the first hydration shell. Likewise, the emergence of red areas peaked at r = 9.5 Å, $\cos(\theta) = 0.33$ and r = 9.5 Å, $\cos(\theta) = -1$ shows an increase in the probability of water molecules with inverted structures in the second hydration shell surrounding the C_{60}. The valleys between the two-hydration shells are lowered. It is indicated by such an analysis that the TIP3P water molecules are rather ordered in the confinement than in the bulk system. The same trend was also observed for the triad solvated by SPC/E water. The change in the probability solvated by SPC/E water is at least 30% greater than TIP3P water.

IV. DISCUSSION

IV.1. Assignment of Thermally Averaged Charges on Triad. It is shown by our simulations that the energy landscape of the triad is broad and shallow in aqueous solution at 350 K. The barriers separating local basins are less than 1 k_BT, indicating that the triad is a very flexible molecule at ambient temperature and the population shift is highly susceptible to subtle changes in solvent parametrization and its surrounding environments. The charge distribution in the triad was strongly affected by its conformational fluctuation. The importance of assigning valid charges for all possible conformations instead of a single static one has been addressed, but it was impeded by a lack of computational power. In an earlier work by Richards,[21] they weighed the atomic charges by including a Boltzmann factor and averaged them over selected conformations. The lack of degeneracy (i.e., density of states) in this model was further improved by the use of MD that allows an ensemble average of multiple configurations.[22] However, its system size for a canonical MD is limited to small and simple monosaccharides. It is insufficient for the triad in our study.

We have improved the algorithm by applying the replica exchange method, which produces a broad phase space of the triad. Given a charge q_i of the ith atom, we have computed an ensemble-averaged charge $\langle q_i \rangle = \int n(E) e^{-E/k_BT} q_i(E)\, dE = \int P(E) q_i(E)\, dE$. The product of the density of the state $n(E)$ and the Boltzmann's factor (e^{-E/k_BT}) gives the probability of configurations $P(E)$ with potential energy E. We have further applied the Metropolis sampling method to select representative conformations to address the appropriate weights of these configurations in the energy landscape at temperature T. By doing so, we have incorporated the impact of thermal fluctuation by combining statistical physics and quantum chemistry where the latter approach is often limited to the computation of charges for small and rigid chemical molecules. Such a reasonable starting point has allowed us to address the charge distribution on the triad by averaging the charges over many "static" configurations in an ensemble so that the variations in structures (conformational fluctuations) were taken into account for the assignment of charges of the triad in solvent under ambient conditions. This is why we have not

dx.doi.org/10.1021/jp212273n | J. Phys. Chem. B 2012, 116, 8460−8473

Table 3. The Energetics between Each Component of the Triad Including C_{60}, Porphyrin (POR), and Carotenoid (CAR), and Two Junction Groups PH1 and PH2 and the Water Molecules in Spherical Shells of 1 Å Measured from the COM of Each Component of the Triad in the Bulk System[a]

radius (Å)			3	4	5	6	7	8
C_{60}	TIP3P	Elec[b]	N/A	N/A	N/A	−0.024 ± 0.014	0.602 ± 0.007	1.025 ± 0.007
		vdW[c]	N/A	N/A	N/A	1.167 ± 0.039	−20.886 ± 0.023	−34.388 ± 0.019
		NonB[d]	N/A	N/A	N/A	1.143 ± 0.042	−20.284 ± 0.024	−33.364 ± 0.020
	SPC/E	Elec	N/A	N/A	N/A	−0.051 ± 0.016	0.784 ± 0.007	1.333 ± 0.007
		vdW	N/A	N/A	N/A	1.160 ± 0.037	−22.034 ± 0.024	−36.288 ± 0.019
		NonB	N/A	N/A	N/A	1.109 ± 0.040	−21.250 ± 0.024	−34.955 ± 0.019
PH1	TIP3P	Elec	−1.249 ± 0.025	−0.516 ± 0.008	−2.187 ± 0.014	−2.784 ± 0.012	−2.863 ± 0.012	−3.008 ± 0.012
		vdW	0.861 ± 0.028	−0.691 ± 0.005	−2.477 ± 0.007	−4.024 ± 0.007	−4.807 ± 0.007	−5.293 ± 0.007
		NonB	−0.388 ± 0.034	−1.208 ± 0.008	−4.664 ± 0.014	−6.809 ± 0.013	−7.670 ± 0.013	−8.301 ± 0.013
	SPC/E	Elec	−1.424 ± 0.025	−0.546 ± 0.008	−2.297 ± 0.014	−3.013 ± 0.012	−3.137 ± 0.012	−3.241 ± 0.012
		vdW	0.905 ± 0.025	−0.707 ± 0.005	−2.592 ± 0.007	−4.226 ± 0.007	−5.030 ± 0.007	−5.541 ± 0.007
		NonB	−0.520 ± 0.031	−1.253 ± 0.008	−4.889 ± 0.015	−7.240 ± 0.013	−8.167 ± 0.012	−8.782 ± 0.012
POR	TIP3P	Elec	−3.123 ± 0.022	−5.456 ± 0.024	−9.656 ± 0.030	−12.811 ± 0.032	−15.366 ± 0.035	−17.831 ± 0.035
		vdW	−1.223 ± 0.010	−2.604 ± 0.010	−5.515 ± 0.013	−9.303 ± 0.015	−13.636 ± 0.016	−18.804 ± 0.018
		NonB	−4.346 ± 0.022	−8.060 ± 0.025	−15.171 ± 0.030	−22.114 ± 0.033	−29.002 ± 0.036	−36.634 ± 0.036
	SPC/E	Elec	−3.375 ± 0.022	−5.874 ± 0.023	−10.236 ± 0.029	−13.659 ± 0.032	−16.349 ± 0.035	−19.062 ± 0.035
		vdW	−1.219 ± 0.010	−2.598 ± 0.010	−5.519 ± 0.013	−9.425 ± 0.014	−13.983 ± 0.016	−19.472 ± 0.017
		NonB	−4.595 ± 0.023	−8.472 ± 0.025	−15.755 ± 0.029	−23.084 ± 0.032	−30.331 ± 0.035	−38.535 ± 0.036
PH2	TIP3P	Elec	−1.372 ± 0.019	−0.768 ± 0.007	−2.061 ± 0.013	−2.688 ± 0.012	−2.708 ± 0.012	−2.768 ± 0.011
		vdW	0.898 ± 0.023	−0.627 ± 0.006	−2.459 ± 0.008	−4.329 ± 0.008	−5.246 ± 0.008	−5.795 ± 0.008
		NonB	−0.474 ± 0.027	−1.394 ± 0.008	−4.521 ± 0.014	−7.017 ± 0.013	−7.954 ± 0.013	−8.563 ± 0.013
	SPC/E	Elec	−1.510 ± 0.019	−0.825 ± 0.008	−2.168 ± 0.013	−2.888 ± 0.012	−2.944 ± 0.012	−2.955 ± 0.012
		vdW	1.003 ± 0.023	−0.609 ± 0.006	−2.529 ± 0.008	−4.513 ± 0.008	−5.455 ± 0.008	−6.026 ± 0.008
		NonB	−0.507 ± 0.027	−1.434 ± 0.008	−4.697 ± 0.014	−7.400 ± 0.013	−8.399 ± 0.013	−8.981 ± 0.013
CAR	TIP3P	Elec	−0.752 ± 0.013	−1.353 ± 0.012	−2.757 ± 0.016	−4.088 ± 0.018	−5.453 ± 0.020	−6.953 ± 0.022
		vdW	−0.689 ± 0.007	−1.839 ± 0.007	−4.837 ± 0.010	−8.443 ± 0.012	−12.425 ± 0.013	−16.688 ± 0.015
		NonB	−1.441 ± 0.013	−3.192 ± 0.014	−7.594 ± 0.018	−12.532 ± 0.021	−17.878 ± 0.023	−23.640 ± 0.026
	SPC/E	Elec	−0.805 ± 0.013	−1.460 ± 0.012	−2.945 ± 0.016	−4.317 ± 0.018	−5.809 ± 0.021	−7.386 ± 0.022
		vdW	−0.706 ± 0.007	−1.889 ± 0.008	−5.020 ± 0.010	−8.770 ± 0.012	−12.932 ± 0.014	−17.389 ± 0.015
		NonB	−1.512 ± 0.014	−3.349 ± 0.014	−7.965 ± 0.018	−13.087 ± 0.021	−18.742 ± 0.023	−24.775 ± 0.026

[a]The triad is solvated by either the TIP3P or SPC/E water. Errors bar are included. The unit is in kcal/mol. [b]Electrostatic potential energy. [c]van der Waals interaction energy. [d]Nonbonded energy.

chosen the set of charges of a static configuration computed by Baruah et al. for our MD simulations.

Regarding the computation of q_i for each of the configuration selected from the ensemble, we have computed the charges of the ground-state triad by using several methods. We have chosen the AM1-BCC methods based on the three arguments below:

First, the Mulliken charges are based on the occupancy of the atomic orbitals and are not capable of accurately reproducing neither the MEP nor even higher electric moments of molecules. Therefore, they are not preferred in the condensed-phase simulations. Second, the RESP charges do reproduce the quantum mechanically calculated molecular electrostatic potential; however, the electrostatic potential fitted atomic charges are dependent[52] on conformations. Particularly, it is most problematic with regard to the charges on buried atoms, which are numerically unstable, and their magnitude can vary significantly.[53] The above problems are manifested in large fluctuations of the RESP charges on the fullerene carbon atoms that are on the order of 1 *e*, while the same carbon atoms experience much smaller variation in charges in the range of 0.1 *e* when calculated by using Mulliken or AM1-BCC methods. Such discrepancy may result from both the conformational dependability of the ESP-fitted charges and the grid sizes for the computation of the electrostatic potential: the grid points for which the quantum mechanical electrostatic potential is evaluated must lay outside the molecular van der Waals surface. As a consequence, buried atoms that are "inside" of the molecule are represented by a relatively smaller number of grid points. This, in turn, leads to numerical instabilities in the fitting procedure that result in poorly defined charges. All the above-mentioned problems with the RESP charges will be even more pronounced in systems with a large conformation and orientation variability that will result in large systematic errors in the computation of charges. In addition, calculations of atomic charges using ESP-fitting or Mulliken population analysis methods can also place heavy demands on computational resources required for quantum mechanical calculations with regard to molecular electrostatic potential and wave function, respectively, especially for large molecules.

Third, AM1-BCC fares better than the other two because it brings the advantages of Mulliken and ESP-fitted charge methods together. The Mulliken population analysis using semiempirical wave function provides AM1 atomic charges that are subsequently corrected using bond charge corrections (BCC)[34,35] parametrized against the HF/6-31G(d) electrostatic potential. The charges calculated with this method show the smallest configurational dependence, and they are not affected by the numerical instabilities encountered in the ESP-fitted charges. Most importantly, among the three methods, only the charges computed by AM1-BCC correctly produce the chemistry of a ground-state triad in which the C_{60} has near zero partial charges.

dx.doi.org/10.1021/jp212273n | J. Phys. Chem. B 2012, 116, 8460−8473

Table 4. The Number of HBs in Spherical Shells of 1 Å Measured from the COM of Each Component of the Triad, Such as C_{60}, POR, and CAR, and Two Junction Groups PH1 and PH2, in the Bulk System Solvated by Either TIP3P or SPC/E Water[a]

radius (Å)		3	4	5	6	7	8
C60	TIP3P	N/A	N/A	N/A	0.000 ± 0.000	14.573 ± 0.033	44.373 ± 0.043
	SPC/E	N/A	N/A	N/A	0.000 ± 0.000	17.239 ± 0.037	51.428 ± 0.045
PH1	TIP3P	0.000 ± 0.000	0.332 ± 0.004	4.451 ± 0.015	13.079 ± 0.022	26.407 ± 0.030	47.644 ± 0.039
	SPC/E	0.000 ± 0.000	0.363 ± 0.004	5.058 ± 0.016	14.868 ± 0.023	29.430 ± 0.030	53.140 ± 0.039
POR	TIP3P	0.015 ± 0.001	0.559 ± 0.005	3.288 ± 0.011	9.407 ± 0.018	22.241 ± 0.028	48.556 ± 0.042
	SPC/E	0.020 ± 0.001	0.630 ± 0.005	3.640 ± 0.011	10.357 ± 0.019	24.790 ± 0.029	54.574 ± 0.043
PH2	TIP3P	0.000 ± 0.000	0.319 ± 0.004	4.571 ± 0.015	14.687 ± 0.024	30.155 ± 0.032	54.283 ± 0.041
	SPC/E	0.000 ± 0.000	0.332 ± 0.004	5.195 ± 0.016	16.733 ± 0.025	33.652 ± 0.032	60.390 ± 0.042
CAR	TIP3P	0.096 ± 0.002	1.285 ± 0.009	6.022 ± 0.017	16.029 ± 0.025	33.058 ± 0.035	58.694 ± 0.045
	SPC/E	0.112 ± 0.003	1.485 ± 0.009	6.968 ± 0.017	18.235 ± 0.025	37.243 ± 0.035	65.962 ± 0.049

[a]The definition of the HB follows the one set by Luzar and Chandler.[54] Error bars are included.

Conclusively, we decided to use the AM1-BCC charges in our simulations.

IV.2. Impact of Small Changes in Water Models on the Triad. We have investigated the impact of solvation on the triad by using two types of water models, TIP3P and SPC/E; both are a three-site water model. The two models have a similar dipole moment (∼ 2.35 D). However, because the HOH angle of SPC/E water is 109.47° assuming an ideal tetrahedral shape while the HOH angle of TIP3P is 104.52° taken from an experimental value, the parameters on the charges and the Lennard-Jones interaction for SPC/E water are slightly greater than TIP3P's. It subtly affects the structure of the HB network surrounding the triad, thus affecting the average conformation of the triad in the bulk and confinement system.

In the bulk systems (PBC), the ensemble structures of the triad solvated by SPC/E water are more compact, shown by a shorter end-to-end distance and a lower shape parameter in Table 2 as a result of stronger order in hydration interactions. In the bulk system, the triad favors a compact structure where the carotenoid bends close to the C_{60}. This phenomena can be also found in topologically complex hydrocarbons where a compact structure is overall more favorable than extended ones.[26] When we compared the distribution of water molecules surrounding the component of the triad in the bulk systems, both water models have shown a higher density distribution around the C_{60} over the porphyrin and the carotenoid (Figure 6).

It was shown that SPC/E water (Figure 7D) is better oriented in clathrate-like structures in the proximity of C_{60} than the TIP3P water (Figure 7A). We have computed the energetics in terms of the electrostatics, van der Waals, and the sum of the two (nonbonded), between the triad and the water molecules in Table 3. The energetics with SPC/E water is slightly more favorable (negative) than that with TIP3P by a fraction of kcal/mol. However, when we computed the number of HBs of a network of water molecules (using the definition of Luzar and Chandler[54]) surrounding the component of the triad in Table 4, the number of HBs of SPC/E water is overwhelmingly greater than that in the TIP3P, particularly when the distance to the COM of the component of the triad, r, exceeds 8 Å. For example, the number of HBs is lost by 15% for C_{60} and 12% for both porphyrin and carotenoid compared to SPC/E water. This is in agreement with prior studies in which the TIP3P water is known to have less structure after the first peak hydration shell.[55] The fact that SPC/E water molecules pack better results in a robust HB network and cancellation of the favorable triad−water interaction in the bulk system. These small differences in the water parametrization dictate the conformations of a highly flexible triad, as seen in other flexible unfolded peptide systems.[56]

IV.3. Confinement Effect on the Triad and Solvation. In the presence of nanosized confinement, the compact state of a topologically complex compound is relatively stabilized over its extended ones because the population of extended configurations is reduced by the restricted space as shown by simple polymer models.[27,57−59] However, when explicit water molecules are included in the simulations, although they make simulations more computational demanding, the solvent-mediated effects on the molecules can be better accounted for with the confining surface.[60,61] Within this framework, it was found that the behavior of a flexible polymeric molecule becomes rather complex[26,62,63] compared to the bulk. It is because hydrophobic solutes in nanosized confinement do not undergo the same oil−water separation (i.e., hydrophobic effect[64]) as the bulk water where the driving force is to maximize the solvent entropy and that the contact area between the hydrophobes and the solvent is minimized. Take methane molecules for an example. Under confinement, methane molecules remain at the surface[47] because it is where the number of HBs in a network of water molecules can be maximized. It becomes increasingly complex when a topologically complex molecule, such as hexane, is considered in a confinement,[26] where an extended structure (*ttt*) is favored over a compact helical one (*gg′g*) in the bulk system.[65]

The triad is a flexible and topologically complex supramolecule where the barrier between basins is at the order of k_BT; thus, its conformation distribution can be easily manipulated by thermal fluctuations of solvent. On top of that, when the presence of confinement is considered, the network of solvent molecules is disrupted and that dictates both the positions of the components in the confinement and its attraction to the wall. The TIP3P water is known for its weak water structure after the first hydration shell. In our study, we have also shown that the presence of confinement is to have a greater impact on the reduction of the number of HBs (Table 4); thus, the attraction of the triad to the wall increases. The numbers of HBs after the first hydration shell are significantly lower for the TIP3P water than the SPC/E water. At 8 Å away from the COM of the triad component, the reduction in HBs can reach 10%. As the size of the confinement reduces, the attraction to the wall grows greater and another free energy minimum appears at the wall. Not only are the positions

dx.doi.org/10.1021/jp212273n | J. Phys. Chem. B 2012, 116, 8460−8473

of the triad in the confinement affected, but also its conformation. In the smallest size of the confinement (SC3.5), multiple parts of the triad can attach to the wall, and that produces a rather short and kinked configuration.

However, when the triad is solvated by SPC/E water, when it was confined in the same nanocapsules, a major population of the triad remains near the interior except for a few atoms at the tip of the carotenoid when it is placed in the smallest confinement. When the sizes of the confinement reduce to SC9.5 and SC6.5, a fully extended triad is populated without attaching to the wall (Table 2). Such drastic differences on the triad whose conformations are highly flexible in solvent has everything to do with the minor differences in the two water models as described in the next paragraph.

Although TIP3P and SPC/E have almost the same value of dipole moment (2.35 D), their HOH angles are parametrized differently. The former is 104.52° modeled after the experimental measurement, and the latter is 109.47° modeled after an ideal tetrahedron. Because the subtle differences in the HOH angle for which SPC/E water is slightly wider, its charges and van der Waals parameters are slightly greater than TIP3P water in order to produce the same value of dipole moment. The impact results in a stronger interaction between the triad and the SPC/E water (Table 3), which favor solubility as well as a robust structure of HB network at further distance away from the solute (Table 4). When confinement conditions are imposed, it greatly disrupts the structure of HB of water surrounding the triad, and that impacts both the conformation distribution of the triad and its position in the confinement. In TIP3P water where the water structure is inherently weak, the triad is more attracted to the surface where most broken HBs reside. It is also shown in similar studies on the confinement effect on large solutes and solvent based on the TIP3P water.[47,62,63]

By contrast, when the triad is solvated by SPC/E water in the confinement, it prefers to a form a rather extended, "chair" configuration with an end-to-end distance very close to the one computed by Baruah et al.[9] rather than the compact ones in the bulk water. It is contributed by both a favorable interaction between the triad and SPC/E water as well as a robust structure of the HB network surrounding the triad molecule. Once the size of confinement is reduced to SC3.5, the tip of the carotenoid is occasionally pinned to the surface, and the conformation of the triad returns to a compact, "boat" structure again.

V. CONCLUSION

We have developed a multiscale approach that integrates quantum chemistry, statistical physics, and MD to determine the thermodynamics behavior of a flexible bioinspired compound triad. We have found that the energy landscape of an ensemble of the triad is shallow, and the barrier separating local minima is merely less than 1 k_BT. Small changes in the parametrizations in the solvent models or the presence of confinement that disturb the network of hydrogen bonding in solvents can drastically shift the population of the triad configuration from one to another as well as its position in a confinement. This study, although based on the ground-state triad, provides better insights into experimental studies on the structural characteristics of the triad in a confined system, such as reverse micelles, and sets a fundamental method for further work on the excited-state of the triad in organic solvent under ambient conditions.

■ ASSOCIATED CONTENT

Supporting Information

Table S1: The atomic indices and the atom types for each component of the triad. A chemical structure is provided in Figure 1A. Table S2: List of the carbon atoms on the carotenoid in classes 1 through 8 as well as their respective colors in Figures S1 and S2. Table S3: The energetics between each component of the triad including C60, POR and CAR, and two junction groups PH1 and PH2 and the water molecules in spherical shells of 1 Å measured from the COM of each component of the triad in various sizes of the confinement. Table S4: The number of HBs in spherical shells of 1 Å measured from the COM of each component of the triad including C60, POR and CAR, and the two junction groups, PH1 and PH2 in various sizes of the confinement. Figure S1: The free energy as a function of position, r, of a carbon atom on the carotenoid from each class in the confinement solvated by either the TIP3P or the SPC/E water model, as well as their respective locations on the carotenoid. Figure S2: The water density, ρwater, as a function of radial distance, r, for each of the carbon atoms on the carotenoid from each class in the bulk system and the confinement solvated by either the TIP3P or the SPC/E water model, as well as their respective locations on the carotenoid. Figure S3. The density of water molecules, ρwater, as a function of distance, r, with respect to the COM of phenyl group 1 (PH1) in A and C, and phenyl group 2 (PH2) in B and D. This information is available free of charge via the Internet at http://pubs.acs.org/.

■ AUTHOR INFORMATION

Corresponding Author

*Address: Department of Physics, University of Houston, Houston, TX 77204, USA. Phone: (713) 743-8358. Fax: (713) 743-3589. E-mail: mscheung@uh.edu.

Notes

The authors declare no competing financial interest.

■ ACKNOWLEDGMENTS

This work was supported by the Department of Energy (DOE), Basic Energy Sciences Grant DE-FG02-10ER16175. M.S.C. thanks Dr. Tunna Baruah for the coordinates of the triad and its charges of an extended triad configuration. M.S.C. also acknowledges the computational sources from the National Energy Research Scientific Computing Center (NERSC), which is supported by the Office of Science of the U.S. Department of Energy under Contract No. DE-AC02-05CH11231, the Texas Advanced Computing Center (TACC), the Texas Learning and computation center (TLC^2), BlueBioU at Rice University, and the University of Houston. G.S. is thankful for the training opportunity given by the Houston Area Molecular Biophysics Predoctoral Training Program (HAMBP). S.M. acknowledges the support of the Provost Undergraduate Research Fellowship at the University of Houston.

■ REFERENCES

(1) Morton, O. *Nature* **2006**, *443*, 19.
(2) Lewis, N. S.; Nocera, D. G. *Proc. Natl. Acad. Sci. U.S.A.* **2006**, *103*, 15729.
(3) Crabtree, G. W.; Lewis, N. S. *Phys. Today* **2007**, *60*, 37.
(4) Liddell, P. A.; Kuciauskas, D.; Sumida, J. P.; Nash, B.; Nguyen, D.; Moore, A. L.; Moore, T. A.; Gust, D. *J. Am. Chem. Soc.* **1997**, *119*, 1400.

(5) Smirnov, S. N.; Liddell, P. A.; Vlassiouk, I. V.; Teslja, A.; Kuciauskas, D.; Braun, C. L.; Moore, A. L.; Moore, T. A.; Gust, D. *J. Phys. Chem. A* **2003**, *107*, 7567.
(6) Gust, D.; Moore, T. A.; Moore, A. L. *Acc. Chem. Res.* **2001**, *34*, 40.
(7) Carbonera, D.; Di Valentin, M.; Corvaja, C.; Agostini, G.; Giacometti, G.; Liddell, P. A.; Kuciauskas, D.; Moore, A. L.; Moore, T. A.; Gust, D. *J. Am. Chem. Soc.* **1998**, *120*, 4398.
(8) Rizzi, A. C.; van Gastel, M.; Liddell, P. A.; Palacios, R. E.; Moore, G. F.; Kodis, G.; Moore, A. L.; Moore, T. A.; Gust, D.; Braslavsky, S. E. *J. Phys. Chem. A* **2008**, *112*, 4215.
(9) Baruah, T.; Pederson, M. R. *J. Chem. Phys.* **2006**, *125*, 164706.
(10) Spallanzani, N.; Rozzi, C. A.; Varsano, D.; Baruah, T.; Pederson, M. R.; Manghi, F.; Rubio, A. *J. Phys. Chem. B* **2009**, *113*, 5345.
(11) Baruah, T.; Pederson, M. R. *J. Chem. Theory Comput.* **2009**, *5*, 834.
(12) Mulliken, R. S. *J. Chem. Phys.* **1955**, *23*, 1833.
(13) Reed, A. E.; Curtiss, L. A.; Weinhold, F. *Chem. Rev.* **1988**, *88*, 899.
(14) Bader, R. *Atoms in Molecules: A Quantum Theory*; Oxford University Press: New York, 1990.
(15) Momany, F. A. *J. Phys. Chem.* **1978**, *82*, 592.
(16) Cox, S. R.; Williams, D. E. *J. Comput. Chem.* **1981**, *2*, 304.
(17) Singh, U. C.; Kollman, P. A. *J. Comput. Chem.* **1984**, *5*, 129.
(18) Bayly, C. I.; Cieplak, P.; Cornell, W.; Kollman, P. A. *J. Phys. Chem.* **1993**, 97.
(19) Williams, D. E.; Yan, J.-M. In *Advances in Atomic and Molecular Physics*; Bates, D. B., Ed.; Academic Press: New York, 1987; Vol. *23*, p 87.
(20) Woods, R. J.; Khalil, M.; Pell, W.; Moffat, S. H.; Smith, V. H. *J. Comput. Chem.* **1990**, *11*, 297.
(21) Reynolds, C. A.; Essex, J. W.; Richards, W. G. *J. Am. Chem. Soc.* **1992**, *114*, 9075.
(22) Basma, M.; Sundara, S.; Calgan, D.; Vernali, T.; Woods, R. J. *J. Comput. Chem.* **2001**, *22*, 1125.
(23) Wang, Q.; Liang, K.-C.; Waxham, M. N.; Cheung, M. S. *PLoS Comput. Biol.* **2011**, *7*, e1002114.
(24) Frenkel, D.; Smit, B. *Understanding Molecular Simulation: From Algorithms to Applications*; Academic Press: New York, 2001.
(25) Baruah, T. Personal Communication, University of Texas, El Paso.
(26) Homouz, D.; Hoffman, B.; Cheung, M. S. *J. Phys. Chem. B* **2009**, *113*, 12337.
(27) Zhang, S.-Q.; Cheung, M. S. *Nano Lett.* **2007**, *7*, 3438.
(28) Sugita, Y.; Okamoto, Y. *Chem. Phys. Lett.* **1999**, *314*, 141.
(29) Case, D. A.; Darden, T. A.; Cheatham, T. E.; Simmerling, C. L.; Wang, J.; Duke, R. E.; Luo, R.; Walker, R. C.; Zhang, W.; Merz, D., et al. *AMBER11*; University of California: San Francisco, CA, 2010.
(30) Wang, J.; Wolf, R. M.; Caldwell, J. W.; Kollman, P. A.; Case, D. A. *J. Comput. Chem.* **2004**, *25*, 1157.
(31) Sanbonmatsu, K. Y.; Garcia, A. E. *Proteins* **2002**, *46*, 225.
(32) Garcia, A. E. *Phys. Rev. Lett.* **1992**, *68*, 2696.
(33) Samiotakis, A.; Homouz, D.; Cheung, M. S. *J. Chem. Phys.* **2010**, *132*, 175101.
(34) Jakalian, A.; Bush, B. L.; Jack, D. B.; Bayly, C. I. *J. Comput. Chem.* **2000**, *21*, 132.
(35) Jakalian, A.; Jack, D. B.; Bayly, C. I. *J. Comput. Chem.* **2002**, *23*, 1623.
(36) Valiev, M.; Bylaska, E. J.; Govind, N.; Kowalski, K.; Straatsma, T. P.; Van Dam, H. J. J.; Wang, D.; Nieplocha, J.; Apra, E.; Windus, T. L.; de Jong, W. *Comput. Phys. Commun.* **2010**, *181*, 1477.
(37) Jorgensen, W. L.; Chandrasekhar, J.; Madura, J.; Impey, R. W.; Klein, M. L. *J. Chem. Phys.* **1983**, *79*, 926.
(38) Berendsen, H. J. C.; Grigera, J. R.; Straatsma, T. P. *J. Phys. Chem.* **1987**, *91*, 6269.
(39) Humphrey, W.; Dalke, A.; Schulten, K. *J. Mol. Graphics* **1996**, *14*, 33.
(40) Phillips, J. C.; Braun, R.; Wang, W.; Gumbart, J.; Tajkhorshid, E.; Villa, E.; Chipot, C.; Skeel, R. D.; Kale, L.; Schulten, K. *J. Comput. Chem.* **2005**, *26*, 1781.
(41) Martyna, G. J.; Tobias, D. J.; Klein, M. L. *J. Chem. Phys.* **1994**, *101*, 4177.
(42) Feller, S. E.; Zhang, Y. H.; Pastor, R. W.; Brooks, B. R. *J. Chem. Phys.* **1995**, *103*, 4613.
(43) Ryckaert, J.-P.; Ciccotti, G.; Berendsen, H. J. C. *J. Comput. Phys.* **1977**, *23*, 327.
(44) Darden, T.; York, D.; Pedersen, L. *J. Chem. Phys.* **1993**, *98*, 10089.
(45) Chodera, J. D.; Swope, W. C.; Pitera, J. W.; Seok, C.; Dill, K. A. *J. Chem. Theory Comput.* **2007**, *3*, 26.
(46) Lamarche, F.; Leroy, C. *Comput. Phys. Commun.* **1990**, *59*, 359.
(47) Vaitheeswaran, S.; Thirumalai, D. *J. Am. Chem. Soc.* **2006**, *128*, 13490.
(48) Dima, R. I.; Thirumalai, D. *J. Phys. Chem. B* **2004**, *108*, 6564.
(49) Cheung, M. S.; Thirumalai, D. *J. Phys. Chem. B* **2007**, *111*, 8250.
(50) Ashbaugh, H. S.; Paulaitis, M. E. *J. Am. Chem. Soc.* **2001**, *123*, 10721.
(51) Raschke, T. M.; Levitt, M. *Proc. Natl. Acad. Sci. U.S.A.* **2005**, *102*, 6777.
(52) Breneman, C. M.; Wiberg, K. B. *J. Comput. Chem.* **1990**, *11*, 361.
(53) Williams, D. E. *Biopolymers* **1990**, *29*, 1367.
(54) Luzar, A.; Chander, D. *Nature* **1996**, *379*, 55.
(55) Mark, P.; Nilsson, L. *J. Phys. Chem. A* **2001**, *105*, 9954.
(56) Florova, P.; Sklenovsky, P.; Banas, P.; Otyepka, M. *J. Chem. Theory Comput.* **2010**, *6*, 3569.
(57) Betancourt, M. R.; Thirumalai, D. *J. Mol. Biol.* **1999**, *287*, 627.
(58) Zhou, H. X.; Dill, K. A. *Biochemistry* **2001**, *40*, 11289.
(59) Friedel, M.; Sheeler, D. J.; Shea, J.-E. *J. Chem. Phys.* **2003**, *118*, 8106.
(60) Setny, P. *J. Chem. Phys.* **2007**, *127*, 054505.
(61) Rao, P. V. G.; Gandhi, K. S.; Ayappa, K. G. *Langmuir* **2007**, *23*, 12795.
(62) Lucent, D.; Vishal, V.; Pande, V. S. *Proc. Natl. Acad. Sci. U.S.A.* **2007**, *104*, 10430.
(63) Tian, J. H.; Garcia, A. E. *J. Am. Chem. Soc.* **2011**, *133*, 15157.
(64) Kauzmann, W. *Adv. Protein Chem.* **1959**, *14*, 1.
(65) Ashbaugh, H. S.; Garde, S.; Hummer, G.; Kaler, E. W.; Paulaitis, M. E. *Biophys. J.* **1999**, *77*, 645.